International Journal of Nanoscience
Vol. 7, Nos. 4 & 5 (2008) 245–253

World Scientific
www.worldscientific.com

BEHAVIOR OF THE CONFINED HARD-SPHERE FLUID WITHIN NANOSLITS: A FUNDAMENTAL-MEASURE DENSITY-FUNCTIONAL THEORY STUDY

MOHAMMAD KAMALVAND and TAHMINEH (EZZAT) KESHAVARZI*
Department of Chemistry
Isfahan University of Technology
Isfahan, Iran, 841568311
**keshavrz@cc.iut.ac.ir*

G. ALI MANSOORI
Departments of Bioengineering
Chemical Engineering and Physics
University of Illinois at Chicago
Chicago, IL 60607-7052, USA
mansoori@uic.edu

Revised 4 August 2008

A property of central interest for theoretical study of nanoconfined fluids is the density distribution of molecules. The density profile of the hard-sphere fluids confined within nanoslit pores is a key quantity for understanding the configurational behavior of confined real molecules. In this report, we produce the density profile of the hard-sphere fluid confined within nanoslit pores using the fundamental-measure density-functional theory (FM-DFT). FM-DFT is a powerful approach to studying the structure and the phase behavior of nanoconfined fluids. We report the computational procedure and the calculated data for nanoslits with different widths and for a wide range of hard-sphere fluid densities. The high accuracy of the resulting density profiles and optimum grid-size values in numerical integration are verified. The data reveal a number of interesting features of hard spheres in nanoslits, which are different from the bulk hard-sphere systems. These data are also useful for a variety of purposes, including obtaining the shear stress, thermal conductivity, adsorption, solvation forces, free volume and prediction of phase transitions.

Keywords: Density-functional theory (DFT); density profile; fundamental-measure DFT (FM-DFT); hard-sphere equation of state; nanoconfined fluid; nanoslit; nanoscience; nanotechnology; phase transition.

1. Introduction

Modern condensed matter theory relies heavily on the knowledge and understanding of the structural and thermodynamic properties of model systems. Among these, the hard-sphere model has been studied extensively and plays an important role in the variational and perturbation theories of condensed matter and phase transitions.[1–3] This is analogous

*Corresponding author.

to the role of the ideal gas in the theory of imperfect gases or the harmonic crystal in solid state physics.[4,5] Today, the variational and perturbation theories are powerful techniques for predicting the structure and behavior of condensed matter. In these theories, properties of the reference model are assumed to be known to an appreciable accuracy and the thermodynamics of the original system is obtained by appropriate adjustment of the potential parameter(s) of the reference system. In most cases, a hard-sphere model system is used, with an appropriately chosen molecular diameter, as the reference model. Furthermore, from the experimental point of view, the hard-sphere model is the simplest colloidal system that can be realized in the laboratory.[5] In summary, the hard-sphere model is remarkable for some important reasons: its configurational integral and its radial distribution function $g(r)$ are independent of temperature; because there are no attractive forces, the only phase transition it has is the fluid–solid transition; the thermodynamic and transport properties of hard spheres depend only on $g(r)$ at the contact point, $g(\sigma)$, where σ is the hard-sphere diameter; the Percus–Yevick (PY) and scaled-particle theories give simple analytic equations for $g(\sigma)$ which are relatively good approximation values; real fluids behave as hard-sphere fluids in the high temperature limit; and, finally, the assumption of pairwise additivity is exact for hard-sphere systems.[3–6]

The behavior of fluids in contact with solid surfaces[7] or confined in small pores[7,8] is of fundamental as well as practical importance. Nanoconfined fluids play an important role in such applications as lubrication, zeolites, catalysis, in gas separation and purification, clay swell, the stability of colloidal systems like emulsions, paints, surface coatings, polymer solutions,[6,9,10] etc. In nanoconfined fluids, the introduction of wall forces, and the competition between fluid–wall and fluid–fluid forces, could lead to interesting fluid behavior and phase changes. These include new kinds of phase transitions not observed in the macroscopic fluid systems, e.g., layering and wetting transitions, as well as shifts in regular bulk transitions (e.g., freezing, gas–liquid, and liquid–liquid).[11] Also, the molecular structure of nanoconfined fluids can differ dramatically from that of macroscopic fluid systems. Consequently, we may not use our knowledge of macroscopic fluid systems when we are dealing with fluids in small confined geometries.[8]

Therefore, due to these complications and the theoretical and technical importance, significant experimental and theoretical efforts have been devoted to this subject. A property of central interest for the theoretical study of nanoconfined fluids is the density distribution of the molecules. That can generally be obtained using computer simulations and/or the classical density-functional theory (DFT). However, a properly administered computer simulation generally could give reliable information about density distribution of the molecules. On the other hand, DFT is a rather powerful approach to studying the structure and the phase behavior of nanoconfined fluids.[12,13] In contrast to slow progress for systems with attractive forces, even for the simple Lennard–Jones (LJ) potential function, DFT has great success for hard spheres.[14] The simplest approximation to DFT is the local density approximation (LDA), which is valid only for weakly inhomogeneous systems, e.g., liquid at a wall; it becomes too crude and one has to use a nonlocal approximation, such as the weighted density approximation (WDA). Therefore, independently, Tarazona[15] and Curtin and Ashcroft[16] constructed weighted-density approaches to DFT for hard-sphere fluid. They wrote the excess free-energy functional as $F_{\text{ex}}[\rho] = \int d\mathbf{r}\rho(\mathbf{r})\psi_{\text{ex}}(\bar{\rho}(\mathbf{r}))$, where the excess free energy per particle ψ_{ex} is evaluated at some coarse-grained or weighted density $\bar{\rho}(\mathbf{r})$, which can be obtained using $\bar{\rho}(\mathbf{r}) = \int d\mathbf{r}'\rho(\mathbf{r}')w(|\mathbf{r}-\mathbf{r}'|)$. The weight function, $w(r,\bar{\rho})$, which determines $\bar{\rho}(\mathbf{r})$, was obtained by requiring the second functional derivative of $-\beta F_{\text{ex}}[\rho]$ to yield an accurate direct correlation function $c^{(2)}(r_{12})$ for the uniform fluid. In practice, this meant enforcing the known PY result for hard spheres.[15,16] Although the approaches proved very successful in a wide variety of applications (including hard-sphere freezing), they are somewhat *ad hoc* in character and their extensions to mixtures are not straightforward. Therefore, Rosenfeld started from a very different perspective.[17] His theory is for hard-sphere mixtures, and is based on a deconvolution of the Mayer f function in terms of four scalar and two vector weight functions.[17] Since his approach is based on the geometrical properties of the spheres, he termed it the "fundamental-measure (FM) theory". Among various versions of DFT, the original FM theory, proposed by Rosenfeld,[17] and some other newer versions[18–23] give very good results for the density profile of hard

spheres in both homogeneous and inhomogeneous conditions.

While there have been extensive investigations into the structure and properties of confined fluids in geometries like cylinders,[21,22,24,25] cavities[26] and specially in contact with a hard wall or within nanoslits,[8,15,16,18–20] there is not any comprehensive report for the density profile of hard-sphere fluid within nanopores. The aim of this research work is to generate the density profile of the hard-sphere fluid within nanoslits with various sizes and in a wide range of hard-sphere densities, using a successful version of the fundamental-measure density-functional theory (FM-DFT). We do this because of the importance of the hard-sphere fluid and its role in the study of real fluids confined in small geometries (nano- and microgeometries), as well as the importance of nanoslit geometry.

The remainder of this paper is organized as follows. In Sec. 2 we briefly describe FM-DFT and we discuss its accuracy for hard-sphere fluid. In Sec. 3, we report the modified FM-DFT results for the density profile of the hard-sphere fluid confined in nanoslit pores and discuss optimum conditions of the calculations and some applications of the data. Finally, in Sec. 4, we report our conclusions and discuss the data obtained.

2. Density-Functional Theory (DFT)

The cornerstone of DFT is that the free energy of an inhomogeneous fluid is a functional of the one-body distribution function $\rho(\mathbf{r})$. Determining the exact form of the free-energy functional is equivalent to calculating the partition function.[12,13] The starting point of DFT is an approximation for the grand canonical free energy, $\Omega[\rho(\mathbf{r})]$, as a functional of $\rho(\mathbf{r})$.[13] $\Omega[\rho(\mathbf{r})]$ can be formulated as a functional of $\rho(\mathbf{r})$ in the context of the grand canonical potential,[14] i.e.,

$$\Omega[\rho(\mathbf{r})] = F[\rho(\mathbf{r})] + \int d\mathbf{r}\rho(\mathbf{r})[V_{\text{ext}}(\mathbf{r}) - \mu]\,, \qquad (1)$$

where $V_{\text{ext}}(\mathbf{r})$ is the external potential and μ is the chemical potential of the inhomogeneous fluid. According to the variational principle, the equilibrium density distribution function of the nonuniform fluid corresponds to the minimum of the grand canonical potential,[14]

$$\frac{\partial\Omega[\rho(\mathbf{r})]}{\partial\rho(\mathbf{r})} = 0\,, \qquad (2)$$

which leads to the Euler–Lagrange equation,[14]

$$\mu - V_{\text{ext}}(\mathbf{r}) = \frac{\partial F[\rho(\mathbf{r})]}{\partial\rho(\mathbf{r})}\,. \qquad (3)$$

The functional $F[\rho(\mathbf{r})]$ is normally split into an ideal and an excess part,[14]

$$F[\rho(\mathbf{r})] = F_{\text{id}}[\rho(\mathbf{r})] + F_{\text{ex}}[\rho(\mathbf{r})]\,, \qquad (4)$$

where $F_{\text{id}}[\rho(\mathbf{r})]$ is the ideal intrinsic Helmholtz free energy, and it is exactly given by[14]

$$F_{\text{id}}[\rho(\mathbf{r})] = k_BT\int d\mathbf{r}\rho(\mathbf{r})\{\ln\Lambda^3\rho(\mathbf{r}) - 1\}\,, \qquad (5)$$

where Λ is the thermal de Broglie wavelength, T is the absolute temperature and k_B is the Boltzmann constant. The Euler–Lagrange equation means that the equilibrium density distribution should satisfy[14]

$$\rho(\mathbf{r})\Lambda^3 = \exp\left(\beta\mu - \beta\frac{\partial F_{\text{ex}}[\rho(\mathbf{r})]}{\partial\rho(\mathbf{r})} - \beta V_{\text{ext}}(\mathbf{r})\right), \qquad (6)$$

or equivalently,[14]

$$\rho(\mathbf{r}) = \rho_b\exp\left(\beta\mu^{\text{ex}} - \beta\frac{\partial F_{\text{ex}}[\rho(\mathbf{r})]}{\partial\rho(\mathbf{r})} - \beta V_{\text{ext}}(\mathbf{r})\right), \qquad (7)$$

where μ^{ex} is the excess chemical potential of the bulk fluid and $\beta = 1/k_BT$. The main approximation in all versions of DFT is an expression for the excess free energy $F_{\text{ex}}[\rho(\mathbf{r})]$ which takes into account the nonideality due to intermolecular interactions. Several approximations have been proposed to accurately describe it during the last two decades.[15–23] Among them, one of the successful approximations is that derived by Rosenfeld (especially for hard-sphere mixtures),[17] which is termed the "fundamental-measure theory FMT". In the FMT, Rosenfeld assumed that the excess Helmholtz-free-energy functional of an inhomogeneous hard-sphere mixture should be expressed in the form of a weighted-density approximation,

$$F_{\text{ex}}^{\text{hs}}[\rho(\mathbf{r})] = k_BT\int d\mathbf{r}\Phi^{\text{hs}}(\mathbf{r})\,, \qquad (8)$$

where $\Phi(\mathbf{r})$ is the excess Helmholtz-energy density that is constructed so that F_{ex} recovers the exact low-density limit and satisfies a certain thermodynamic requirement. The resulting functional generates $c^{(2)}(r_{12})$, which in the Rosenfeld functional is identical to those of the PY theory.[19,20] According

to Rosenfeld's approach, $\Phi(\mathbf{r})$ is a function of the weighted averages of the density distribution function, $\rho_i(\mathbf{r})$:

$$\sum_i \int d\mathbf{r}' \rho_i(\mathbf{r}') w_i^{(\alpha)}(\mathbf{r}-\mathbf{r}') \equiv \sum_i n_{\alpha,i}(\mathbf{r}) \,, \qquad (9)$$

Rosenfeld's FMT has six weight functions, containing four scalar and two vector weight functions, as follows:

$$\begin{aligned} w_i^3(\mathbf{r}) &= \theta(R_i - r) \,, \\ w_i^2(\mathbf{r}) &= \delta(R_i - r) = 4\pi R_i w_i^1(\mathbf{r}) = 4\pi R_i^2 w_i^0(\mathbf{r}) \,, \\ \mathbf{w}_i^2(\mathbf{r}) &= \frac{\mathbf{r}}{|\mathbf{r}|}\delta(R_i - r) = 4\pi R_i \mathbf{w}_i^1(\mathbf{r}) \,, \end{aligned} \qquad (10)$$

where R_i is the hard-sphere radius, $\delta(r)$ the Dirac delta function and $\theta(r)$ the Heaviside step function. According to Rosenfeld's, FMT, $\Phi(\mathbf{r})$ has the expression

$$\Phi = \Phi_S + \Phi_V \,, \qquad (11)$$

where[19,20]

$$\begin{aligned} \Phi_S[\{n_\alpha(\mathbf{r})\}] = &- n_0 \ln(1-n_3) \\ &+ \frac{n_1 n_2}{1-n_3} + \frac{1}{24\pi}\frac{n_2^3}{(1-n_3)^2} \,, \end{aligned} \qquad (12)$$

$$\Phi_V[\{n_\alpha(\mathbf{r})\}] = -\frac{\mathbf{n}_1 \cdot \mathbf{n}_2}{1-n_3} - \frac{1}{8\pi}\frac{n_2(\mathbf{n}_2 \cdot \mathbf{n}_2)}{(1-n_3)^2} \,. \qquad (13)$$

In the above expressions, Φ_S is the scalar part of $\Phi(\mathbf{r})$ and is recognized as the scaled particle theory (SPT) excess free-energy density of the uniform hard-sphere mixture,[18] and Φ_V is the vector part of $\Phi(\mathbf{r})$ which vanishes in the limit of uniform density.[19,20]

One of the inaccuracies of the original Rosenfeld FMT is that its basis bulk-fluid equation of state is the PY compressibility equation equivalent to the SPT.[19,20] Thus for a pure hard-sphere fluid, the contact values (or pressure) are overestimated in comparison with the Monte Carlo simulation results.[19,20] Some years after Rosenfeld's publication of the original FMT, Tarazona introduced a tensor-like weight function into the free-energy density functional[23] and modified the original FMT. Later, Roth *et al.*[20] and Yu and Wu[19] separately but simultaneously formulated a new free-energy functional, termed the "modified FMT",[19,20] based on the Mansoori–Carnahan–Starling–Laland (MCSL) hard-sphere mixture equation of state.[27] Their results showed improvements on those from the original FMT. In the modified fundamental-measure theory (mFMT), $\Phi = \Phi_S + \Phi_V$, which is the same as in the original FMT though the expressions for Φ_S and Φ_V are replaced by the expressions[19,20]

$$\begin{aligned} \Phi_S[\{n_\alpha(\mathbf{r})\}] = &- n_0 \ln(1-n_3) + \frac{n_1 n_2}{1-n_3} \\ &+ \left[\frac{1}{36\pi n_3^2}\ln(1-n_3) \right. \\ &\left. + \frac{1}{36\pi n_3 (1-n_3)^2}\right] n_2^3 \,, \end{aligned} \qquad (14)$$

$$\begin{aligned} \Phi_V[\{n_\alpha(\mathbf{r})\}] = &- \frac{\mathbf{n}_1 \cdot \mathbf{n}_2}{1-n_3} - \left[\frac{1}{12\pi n_3^2}\ln(1-n_3) \right. \\ &\left. + \frac{1}{12\pi n_3 (1-n_3)^2}\right] n_2 (\mathbf{n}_2 \cdot \mathbf{n}_2) \,. \end{aligned} \qquad (15)$$

As with the original FMT, the vector part of $\Phi(\mathbf{r})$ vanishes in the limit of the uniform fluid.[19,20] Because the MCSL equation of state is more accurate than the PY compressibility equation, there is a clear improvement of mFMT results over the original FMT for representing thermodynamic properties of bulk hard-sphere fluids.[19,20] Also, for a one-component hard-sphere fluid, mFMT represents the density profile quite accurately, without the need to introduce into it the tensor-weighted density of Tarazona.[19,20]

Before presenting our results for nanoslit density profiles, we report the results of some theories for the radial distribution function (RDF) of a macroscopic hard-sphere fluid system to demonstrate the reliability of the mFMT results. Figure 1 shows the RDF of a macroscopic hard-sphere fluid

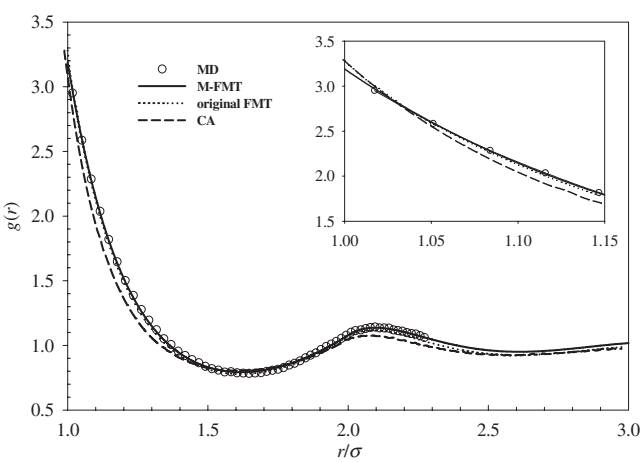

Fig. 1. Radial distribution function of a hard-sphere fluid obtained by CA-weighted DFT,[16] original FMT and mFMDFT in comparison with results of Monte Carlo simulation.[28]

at the moderate reduced density of $\rho\sigma^3 = 0.7$ obtained by the Monte Carlo simulation,[28] weighted DFT of Curtin and Ashcroft (CA),[16] original FM-DFT and mFM-DFT. In this figure, the higher accuracy of the RDF obtained by mFM-DFT is quite clear.

In the next section, we present and discuss calculation of the density profile of the hard-sphere fluid confined in various nanoslit pores using mFM-DFT.

3. Density-Profile Calculation

For the case of the one-component hard-sphere fluid in contact with a hard wall or confined in a nanoslit pore, the external potential and density profile vary only in the z direction, i.e., $\rho(\mathbf{r}) = \rho(z)$ and $V_{\text{ext}}(\mathbf{r}) = V_{\text{ext}}(z)$, where z is the perpendicular distance from the origin of the slit. For the case of slit geometry the external potential is given by

$$V_{\text{ext}}(\mathbf{r}) = V_{\text{ext}}(z) = \begin{cases} \infty & z \le -\dfrac{H}{2} \text{ and } z \ge \dfrac{H}{2}\,, \\ 0 & -\dfrac{H}{2} < z < \dfrac{H}{2}\,, \end{cases} \tag{16}$$

where H is the width of the nanoslit pore. In this case, the weighted densities are[19,20]

$$\begin{aligned} n_0(z) &= \frac{2n_1(z)}{\sigma}\,, \\ n_1(z) &= \frac{n_2(z)}{2\pi\sigma}\,, \\ n_2(z) &= \pi\sigma \int_{-\sigma/2}^{+\sigma/2} \rho(z+z')dz'\,, \\ n_3(z) &= \pi \int_{-\sigma/2}^{+\sigma/2} \rho(z+z') \left[\frac{\sigma^2}{4} - z'^2\right] dz'\,, \\ \mathbf{n}_1(z) &= \frac{\mathbf{n}_2(z)}{2\pi\sigma}\,, \\ \mathbf{n}_2(z) &= 2\pi\mathbf{e}_z \int_{-\sigma/2}^{+\sigma/2} \rho(z+z')z'dz'\,, \end{aligned} \tag{17}$$

where $\mathbf{e}_z$ is the unit vector in the z direction.[19,20] The equilibrium density profile of the hard-sphere fluid in a nanoslit pore, $\rho(z)$, is obtained by minimization of the grand canonical potential or iterative solution to Eq. (7). The excess chemical potential in this equation can be obtained via the MCSL equation of state at the pure hard-sphere limit,[27] which is equivalent to the Carnahan–Starling equation of state,[29]

$$\beta\mu^{\text{ex}} = \eta\frac{8 - 9\eta + 3\eta^2}{(1-\eta)^3}\,, \tag{18}$$

where $\eta = (\pi/6)\rho\sigma^3$ is the packing fraction. Equation (7) is solved using the Picard iterative method.[14] In the calculations, all integrals are evaluated using the trapezoidal rule. Therefore, it is clear that the step size Δz affects the accuracy of the results, i.e., selection of appropriate step size is important when one is performing quantitative calculations. In other literature, different step sizes (from $0.1\,\sigma$ to $0.005\,\sigma$) are reported.[30,31] However, it is not clear what step size is the optimum value for accurate calculation of the density profile. For selection of the optimum value of the step size, we obtained the density profile of the hard-sphere fluid in contact with a hard wall with different step sizes from $0.1\,\sigma$ to $0.0008\,\sigma$ for a wide range of fluid densities. Our results showed that the contact value was significantly underestimated when the step size was greater than $0.00125\,\sigma$. Figure 2 shows the contact value of the density profile $\rho(0)$ versus grid point number $\sigma/\Delta z$ at the reduced bulk density of $\rho\sigma^3 = 0.7$. This figure indicates that to obtain accurate results the grid point number should be greater than 800, or $\Delta z < 0.00125\sigma$. Therefore, to be on the safe side, we performed all of the calculations using $\Delta z = 0.001\,\sigma$.

In the Picard iterative method for solving the Euler–Lagrange equation, a suitable initial guess for $\rho(z)$ is the bulk density, ρ, at low density or by using

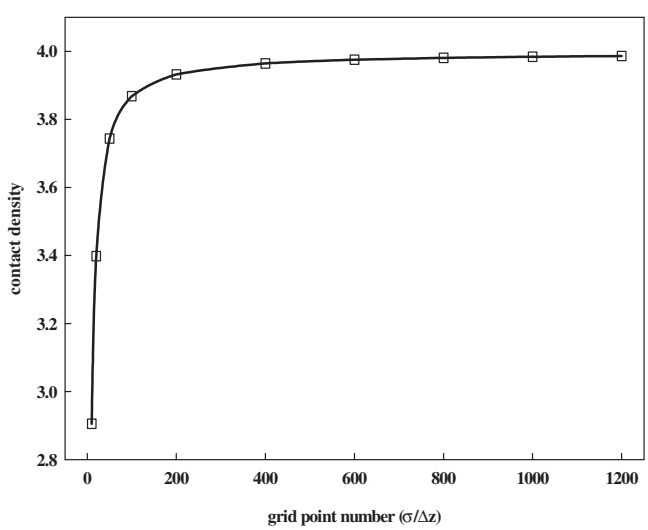

Fig. 2. Contact value of the hard-sphere fluid density profile $\rho(0)$ versus grid point number $\sigma/\Delta z$ for the reduced bulk density $\rho\sigma^3 = 0.7$.

the $\rho(z)$ of a confined fluid at a lower density as input. The new estimate for $\rho(z)$ is then obtained from Eq. (7). This iterative process is repeated until a converged density distribution is obtained. The number of iterations to reach convergence depends on the initial guess, step size, system size (distance between the two slit walls), and more heavily on the bulk density as well as the required precision. In our calculations, the iteration is repeated until the change in the density profile at each point is smaller than $0.0001\,\sigma^3$.

In Fig. 3 the density profile of hard-sphere fluid in contact with a hard wall, obtained by mFM-DFT and compared with the MC simulation results for a reduced bulk density of $\rho\sigma^3 = 0.813$, is reported. The good accuracy of the mFM-DFT results in all ranges of z is clear from this figure. In Fig. 4 mFM-DFT and the MC simulation results for the contact value of the hard-sphere fluid within the nanoslit pore at a number of bulk densities are shown. According to this figure, the maximum percentage error is 16% for $\rho\sigma^3 = 0.8$ and $H = 2\sigma$; in other states, this error is smaller than 4%. It is noticeable that the error for $\rho(z)$ at $z > \sigma/2$ is not significant in all densities and for all pore widths (see Fig. 3). This indicates that the integration error of the density profile is negligible. For example, in the calculation of the reduced average density of the nanoslit, $\bar{\rho}^*$, the maximum relative error for $\rho\sigma^3 = 0.8$ and $H = 2\sigma$ is 1.6%, which is not significant. The reduced average density inside the slit pore is given by[32]

$$\bar{\rho}* = \frac{1}{H}\int_{-H/2}^{+H/2} \rho(z)\sigma^3 dz\,. \tag{19}$$

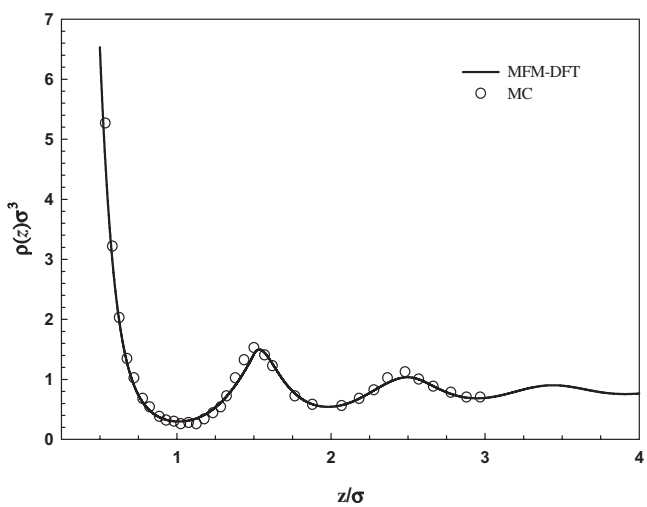

Fig. 3. Comparison of the hard-sphere reduced-density profiles obtained by mFMT-DFT and simulation results[19,20] for $\rho\sigma^3 = 0.813$.

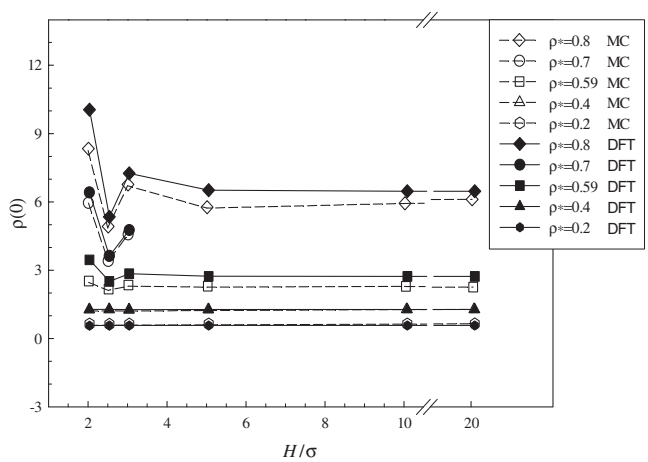

Fig. 4. Comparison of contact value $\rho(0)$ of hard-sphere fluid within different slit pores at some densities.

The values of the reduced average densities obtained by the Monte Carlo simulation and mFM-DFT methods for a number of states are reported in Table 1. According to this table, the DFT calculation produces very accurate results. Therefore, the accuracy of data in the calculation of any thermodynamic property of real fluids, which is related to the integral of the density profile in the full range, is satisfactory.

For example, the shear stress (hence viscosity) and heat flux (hence thermal conductivity) for an inhomogeneous fluid may be formulated using these local densities. In the case of nanofluids, one of the main causes of the enhanced thermal conductivity is the formation of a nanolayer around the nanoparticle,[33,34] which can be studied accurately using the density profile of the nanofluid near a hard wall or around a colloidal particle. The plate–fluid interfacial tension and the excess adsorption are some other quantities, which may be formulated using these local densities.[35] Also, using these density-profile data, the variational and perturbation approaching the equation of state for nanoconfined fluids[8] may be formulated. The other possible application of these data is calculating the free volume of the hard-sphere fluid confined within nanoslit pores, which is a very useful quantity for estimating the excess entropy of the nanoconfined hard-sphere fluid. In addition, using these data, one can formulate the normal pressure for a fluid confined within a nanoslit pore.

Phase transitions in a nanoconfined fluid are different from those in a nonconfined fluid. These transitions may happen at a special density and at any pore size, and are predictable via the

Table 1. Comparison of the reduced average density $\bar{\rho}*$ of the hard-sphere fluid as a function of the reduced slit width H/σ and at various reduced bulk densities as obtained by mFM-DFT and compared with the Monte Carlo simulation.[32]

	$\rho_b = 0.2$		$\rho_b = 0.4$		$\rho_b = 0.59$		$\rho_b = 0.8$	
H/σ	MC	DFT	MC	DFT	MC	DFT	MC	DFT
2	0.124 ± 0.015	0.126	0.286 ± 0.015	0.283	0.475 ± 0.016	0.464	0.727 ± 0.008	0.715
2.5	0.139 ± 0.014	0.141	0.320 ± 0.014	0.317	0.501 ± 0.011	0.497	0.671 ± 0.007	0.679
3	0.149 ± 0.012	0.151	0.330 ± 0.013	0.327	0.514 ± 0.011	0.510	0.734 ± 0.006	0.735
5	0.168 ± 0.010	0.171	0.361 ± 0.010	0.357	0.549 ± 0.010	0.543	0.748 ± 0.008	0.755
10	0.183 ± 0.008	0.183	0.382 ± 0.007	0.379	0.575 ± 0.005	0.566	0.776 ± 0.009	0.777
20	0.190 ± 0.006	0.190	0.394 ± 0.006	0.387	0.585 ± 0.005	0.578	0.777 ± 0.010	0.777

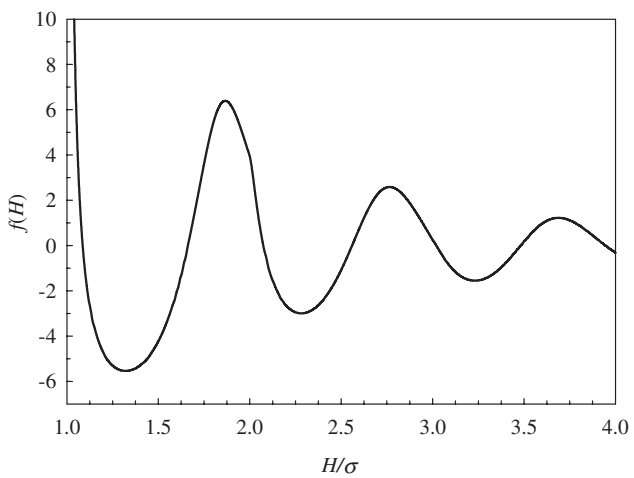

Fig. 5. Solvation force of the hard-sphere fluid confined in nanoslit pores at the reduced bulk density $\rho\sigma^3 = 0.9$.

examination of the thermodynamic potential function of the system at various densities and pore sizes. Also, a phase transition is predictable by consideration of the solvation force[36] at different bulk densities and pore sizes. The solvation force is given by the exact statistical-mechanical formula for a confined hard-sphere fluid,[13]

$$f(H) = k_B T(\rho_H(0) - \rho_\infty(0)), \qquad (20)$$

where $\rho_H(0)$ is the fluid density in contact with each wall in the confined system and $\rho_\infty(0)$ is the corresponding quantity for infinite wall separation. Figure 5 shows the solvation force of the hard-sphere fluid, which is proportional to $\rho(z)$ at contact, at the reduced bulk density of $\rho\sigma^3 = 0.9$ confined in nanoslits with different sizes.

Such data could have interesting applications in statistical mechanics and kinetic theory of dense fluids for prediction of the thermodynamic and transport properties. Therefore, it is necessary to have the density profile in a wide range of fluid densities and pore sizes. Figure 6 shows a part of these data for a confined hard-sphere fluid. As is clear from this figure, when H increases to certain multiples of the hard-sphere diameter, practically $\rho(z)$ of the confined fluid inside the nanoslit becomes the same as the fluid $\rho(z)$ near a hard wall. Therefore, at each density, we obtain $\rho(z)$ from $H = 1.5\,\sigma$ up to H, where $\rho(z)$ becomes identical to the density profile of the hard-sphere fluid near a hard wall.

4. Conclusions and Discussion

Because of the increasing importance of studying the structure and properties of confined fluids in nanoscopic pores and the central role of the hard-sphere model in the theoretical study of real condensed fluids, we have reported here detailed density profiles of the hard-sphere fluid confined in nanoslit pores with different sizes and in a wide range of fluid densities. These data are calculated using a relatively accurate fundamental-measure density-functional theory. Our results are accurate enough to be used for various future calculations, such as predicting phase transitions; calculating reduced average density; obtaining equations of state and estimating the excess entropy — just to mention a few. The maximum error of the reported densities profiles is for the contact value at high densities and small pore widths; however, the error of $\rho(z)$ at $z > \sigma/2$ is negligible for all densities.

Acknowledgments

The authors acknowledge the financial support from the Isfahan University of Technology Research Council and the University of Illinois at Chicago Graduate College.

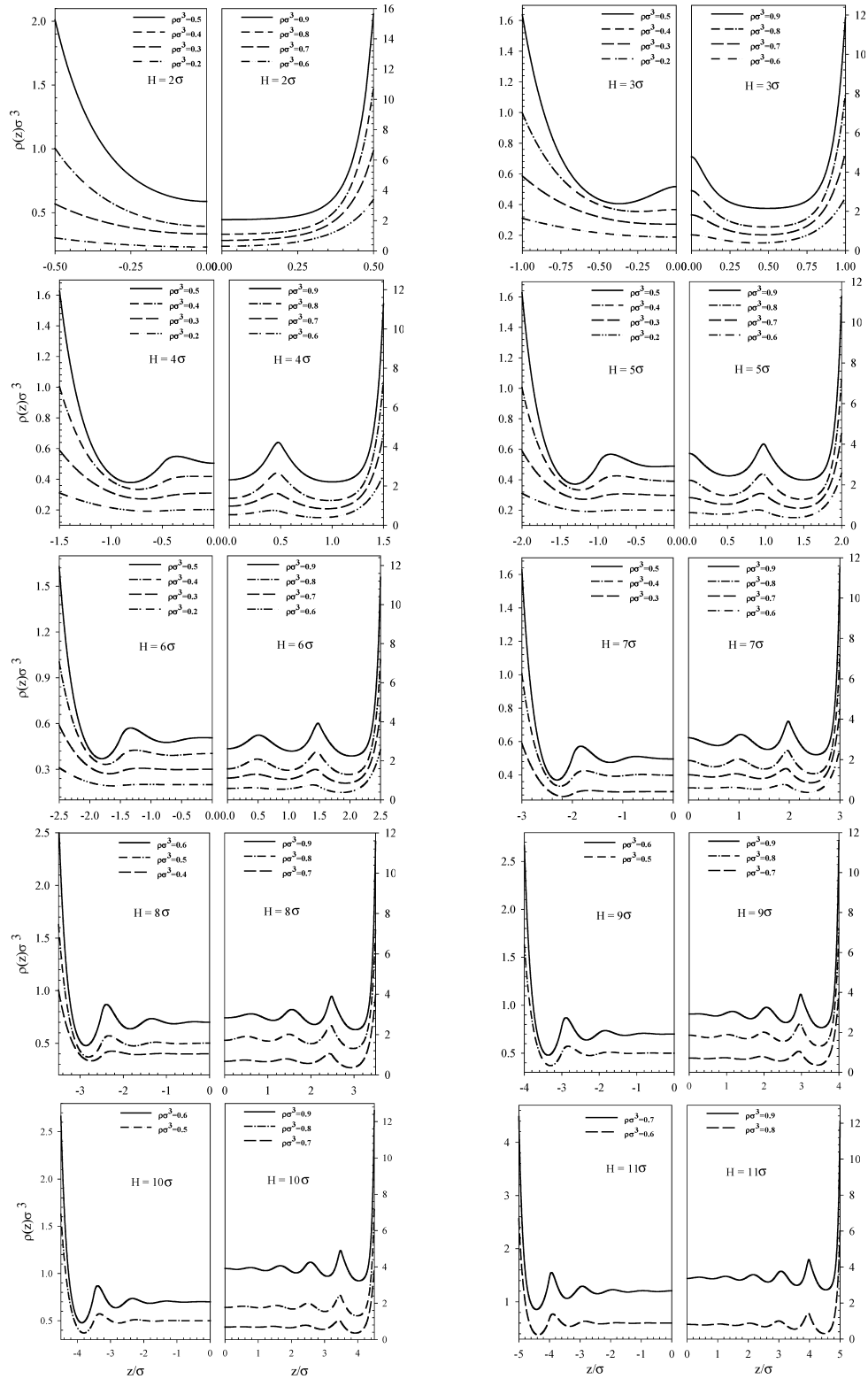

Fig. 6. Density profile of a hard-sphere fluid confined within nanoslit pores with various widths. To enhance visual clarity, the density profile for $\rho\sigma^3 = 0.7$ has been shifted upward by 0.5, for $\rho\sigma^3 = 0.8$ by 1 and for $\rho\sigma^3 = 0.9$ by 2 for slits with $H = 2$–7σ; the density profile for $\rho\sigma^3 = 0.6$ shifted upward by 0.1, for $\rho\sigma^3 = 0.8$ by 1 and for $\rho\sigma^3 = 0.9$ by 2 for slits with $H = 8$–9σ; the density profile for $\rho\sigma^3 = 0.6$ shifted upward by 0.1, for $\rho\sigma^3 = 0.8$ by 1 and for $\rho\sigma^3 = 0.9$ by 3 for slits with $H = 10\sigma$; and the density profile for $\rho\sigma^3 = 0.7$ shifted upward by 0.5 and for $\rho\sigma^3 = 0.9$ by 2.5 for slits with $H = 11\sigma$. For the numerical-data source of this figure, contact M. Kamalvand, m_kamalvand@ch.iut.ac.ir; m_kamalvand@yahoo.com.

References

1. F. Kermanpour, G. A. Parsafar and G. A. Mansoori, *Int. J. Thermophys.* **1**, 187 (2004).
2. E. Z. Hamad and G. A. Mansoori, *Fluid Phase Equil.* **37**, 255 (1987).
3. A. Tani, D. Henderson, J. A. Barker and C. E. Hecht, *Mol. Phys.* **48**, 863 (1983).
4. J. L. Barrat and J. P. Hansen, *Basic Concepts for Simple and Complex Liquids* (Cambridge University Press, 2003).
5. J. M. Haile, *Molecular Dynamics Simulation* (Wiley-Interscience, 1997).
6. G. A. Mansoori, *Principles of Nanotechnology: Molecular-Based Study of Condensed Matter in Small Systems* (World Scientific, 2005).
7. N. M. Tukur, E. Z. Hamad and G. A. Mansoori, *J. Chem. Phys.* **110**, 3463 (1999).
8. E. Keshavarzi, R. Sohrabi and G. A. Mansoori, *J. Comput. Theor. Nanosci.* **3**, 134 (2006).
9. G. A. Mansoori, *Condens. Matter Phys.* **8**, 389 (2005).
10. E. Keshmirizadeh, H. Modarress, A. Eliassi and G. A. Mansoori, *Eur. Polymer J.* **39**, 1141 (2003).
11. B. D. Swanson, H. Stragier, D. J. Tweet and L. B. Sorensen, *Phys. Rev. Lett.* **62**, 909 (1989).
12. K. Esfarjani and G. A. Mansoori, Statistical mechanical modeling and its application to nanosystems, *Handbook of Theoretical and Computational Nanotechnology* (Am. Sci., Stevenson Ranch, California, 2005).
13. D. Henderson, *Fundamentals of Inhomogeneous Fluids* (Dekker, New York, 1991).
14. Y. Tang and J. Z. Wu, *J. Chem. Phys.* **119**, 7388 (2003).
15. P. Tarazona, *Phys. Rev. A* **31**, 2672 (1985).
16. W. A. Curtin and N. W. Ashcroft, *Phys. Rev. A* **32**, 2909 (1985).
17. Y. Rosenfeld, *Phys. Rev. Lett.* **63**, 980 (1989).
18. E. Kierlik and M. L. Rosinberg, *Phys. Rev. A* **42**, 3382 (1990).
19. X. Yu and J. Z. Wu, *J. Chem. Phys.* **117**, 10156 (2002).
20. R. Roth, R. Evans, A. Lang and G. Kahl, *J. Phys.: Condens. Matter* **14**, 12063 (2002).
21. A. Malijevsky, *J. Chem. Phys.* **125**, 194519 (2006).
22. A. Malijevsky, *J. Chem. Phys.* **126**, 134710 (2007).
23. P. Tarazona, *Phys. Rev. Lett.* **84**, 694 (2000).
24. S. F. Gerstenmaier, F. J. Blas, J. B. Avolas and L. F. Vega, *J. Chem. Phys.* **118**, 830 (2003).
25. A. Gonzalez, J. A. White, F. L. Roman and S. Velasco, *J. Chem. Phys.* **125**, 64703 (2006).
26. M. Moradi and M. K. Tehrani, *Phys. Rev. E* **63**, 21202 (2001).
27. G. A. Mansoori, N. F. Carnahan, K. E. Starling and T. W. Laland, Jr., *J. Chem. Phys.* **54**, 1523 (1971).
28. B. J. Alder, S. P. Frankel and V. A. Lewinson, *J. Chem. Phys.* **23**, 417 (1955).
29. N. F. Carnahan and K. E. Starling, *J. Chem. Phys.* **51**, 635 (1969).
30. K. Jagannathan and A. Yethiraj, *J. Chem. Phys.* **116**, 5976 (2002).
31. Y. X. Yu, F. Q. You, Y. Tang, G. H. Gao and Y. G. Li, *J. Phys. Chem. B.* **110**, 334 (2006).
32. R. Kjellander and S. Sarman, *J. Chem. Soc. Faraday Trans.* **87**, 1869 (1991).
33. S. M. S. Murshed, K. C. Leong and C. Yang, *Int. J. Nanosci.* **5**, 23 (2006).
34. J. Sabbaghzadeh and S. Ebrahimi, *Int. J. Nanosci.* **6**, 45 (2007).
35. D. Fu, *J. Chem. Phys.* **124**, 164701 (2006).
36. K. G. Ayappa and C. Ghatak, *J. Chem. Phys.* **117**, 5373 (2002).